NASA TM-83144

NASA Technical Memorandum 83144

NASA-TM-83144 19810017959

QUALITATIVE COMPARISON OF CALCULATED TURBULENCE RESPONSES WITH WIND-TUNNEL MEASUREMENTS FOR A DC-10 DERIVATIVE WING WITH AN ACTIVE CONTROL SYSTEM

BOYD PERRY, III

JUNE 1981

NASA
National Aeronautics and Space Administration
Langley Research Center
Hampton, Virginia 23665

QUALITATIVE COMPARISON OF CALCULATED TURBULENCE RESPONSES WITH WIND-TUNNEL MEASUREMENTS FOR A DC-10 DERIVATIVE WING WITH AN ACTIVE CONTROL SYSTEM

Boyd Perry, III*
NASA Langley Research Center
Hampton, Virginia

Abstract

This paper presents comparisons of analytically-predicted and experimental turbulence responses of a wind-tunnel model of a DC-10 derivative wing equipped with an active control system. The active control system was designed for the purpose of flutter suppression, but it had the additional benefit of alleviating gust loads (wing bending moment) by about 25 percent. Comparisons of various wing responses are presented for variations in active-control-system parameters and tunnel speed. The analytical turbulence responses were obtained using DYLOFLEX, a computer program for dynamic loads analyses of flexible airplanes with active controls. In general, the analytical predictions agreed reasonably well with the experimental data.

Nomenclature

$\{C\}$	generalized aerodynamic vector due to gust
$\bar{C},\bar{\bar{C}}$	load coefficients due to gust aerodynamics
f	frequency, Hz
$H_R(f)$	frequency response function of response R
K_g	fraction of nominal gain
K_p	phase-control-filter gain
M_b	bending moment in the plane of the wing about axis perpendicular to wing spar
$[M_1],[M_2],[M_3]$	generalized structural stiffness, damping, and mass matrices
$[M_4],[M_5]$	generalized aerodynamic matrices due to motion
$L\bar{M}_3J,L\bar{\bar{M}}_3J$	load coefficient vectors due to inertia
$L\bar{M}_4J,L\bar{\bar{M}}_4J,$ $L\bar{M}_5J,L\bar{\bar{M}}_5J$	load coefficient vectors due to motion aerodynamics
$\{q\}$	vector of generalized coordinates
s	Laplace variable
T	torsion about wing spar
w_g	vertical gust velocity
$\ddot{z}$	vertical acceleration, positive down
δ_a	aileron deflection, positive trailing edge down
δ_c	commanded actuator rotation
σR	root-mean-square value of response R
τ	phase-control-filter time constant
ϕ	phase angle, degrees
$L\phi J$	vector of normalized modal deflections
$\Phi_R(f)$	power spectral density function of response R
$\hat{\Phi}_R(f)$	normalized power spectral density function of response R
$\Phi_{w_g}(f)$	power spectral density function of vertical gust velocity

Abbreviations

ACS	active control system
FM	frequency modulated
psd	power spectral density
rms	root mean square

A dot over a quantity represents time derivative.

Introduction

As part of the NASA Aircraft Energy Efficiency Program, the NASA Langley Research Center entered into a cooperative study with the McDonnell Douglas Corporation to test two NASA-developed control laws for active flutter suppression on an aeroelastic wind-tunnel model of a DC-10 derivative wing.[1] It was determined by analysis prior to the wind-tunnel tests that, in addition to suppressing flutter, one of the control laws was also effective in reducing wing bending moments due to turbulence. The analysis which predicted the reduction in wing bending moment was performed using DYLOFLEX, a computer program system for dynamic loads analyses of flexible airplanes with active controls.[2,3] In order to verify that the control law would in fact alleviate gust loads, turbulence-response experiments were added to the wind-tunnel test plan. These wind-tunnel tests provided an opportunity to validate the analysis by comparing analytical predictions with experimental measurements.

The purpose of this paper is to present a status report on the comparison of the analytically-predicted and experimental turbulence responses of this DC-10 wind-tunnel model equipped with a NASA-designed active control system. Normalized power spectral density functions and root-mean-square values of wing responses to tunnel turbulence are presented for variations in active control system parameters and tunnel speed.

Wind-Tunnel Model

The wind-tunnel model used in this investigation was an aeroelastically-scaled semispan model of a DC-10 derivative wing. Detailed descriptions of the geometry and construction of the model are found in Refs. 1 and 4. A photograph of the model mounted in the wind tunnel is presented in Fig. 1.

*Aerospace Engineer, Active Controls Group, Loads and Aeroelasticity Division.

Instrumentation

Figure 2 presents a sketch of the wing planform illustrating the location and type of instrumentation used for the experimental investigation. The dashed line represents the wing spar. The 1.24-m dimension is the model semispan extended to the imaginary vehicle centerline. Strain gage bridges were located in pairs (+ symbols) at approximately the 48 percent and the 78 percent semispan stations. The inboard bridge in each pair was aligned to measure the torsion about the wing spar; the outboard bridge in each pair was aligned to measure the bending moment in the plane of the wing about an axis perpendicular to the wing spar. An accelerometer (• symbol) was mounted on the wing spar at the 88 percent semispan station. It measured vertical acceleration and was used as the feedback sensor for the active control system. A rotary potentiometer (■ symbol) was used to measure aileron deflection.

Active Control System

The active control system (ACS) used in this investigation is represented by the block diagram in Fig. 3. The box labeled "DC-10 wing" represents the wind-tunnel model. The quantity "w_g" represents a disturbance input from the vertical component of wind-tunnel turbulence. Vertical acceleration ($\ddot{z}$) is measured at the 88 percent wing semispan station. A phase-control filter was included to permit entering a "pure" phase angle. By properly choosing the quantities τ and K_p, a phase lead or lag of known amount, ϕ, may be introduced at a given frequency without introducing a change in the gain of the system. "Nominal" phase is $\phi = 0°$. A washout filter was included to attenuate any low-frequency feedback signals and to eliminate any DC signals. The ACS filter is the NASA-developed control law referred to as "Control Law 1" in Ref. 1. (Reference 1 describes the manner in which this control law was synthesized and compares the predicted and actual flutter-suppression performance of this ACS.) The quantity K_g is a normalized gain. It was continuously variable and had a value of unity for "nominal" gain, and a value of zero for system off. The actuator transfer function in Fig. 3 was obtained from an approximation to the measured actuator frequency response.

Wind-Tunnel Tests

The wind-tunnel tests were conducted in the Douglas Long Beach Wind Tunnel (DLBWT) at Long Beach, CA.

History

This wind-tunnel model was tested in the DLBWT on three different occasions. The first was without NASA participation and the results of this test are reported in Ref. 4. The second and third were with NASA participation. The second test was devoted almost exclusively to flutter testing. However, six turbulence-response runs were made with the active control system off and on (nominal gain and phase only) at each of three tunnel speeds. The third test involved flutter testing and turbulence-response testing in roughly equal amounts. This paper deals primarily with the turbulence-response runs made during the third test.

The flutter tests were conducted first. Flutter speeds were measured for many combinations of the active control system gain (K_g) and phase angle (ϕ). On the basis of the flutter tests, stable combinations of gain, phase angle and tunnel speed were then selected for the turbulence-response tests.

Tunnel Turbulence

In order to perform the turbulence-response wind-tunnel tests, turbulence had to be created in the test section. This turbulence was created by installing a canvas "banner" across the width of the tunnel about 5 m upstream of the test section. The flapping of the banner, while the tunnel was running, created random fluctuations in velocity.

Power spectral density functions (psd's) of the vertical component of these velocity fluctuations at tunnel speeds of 30.87, 38.58 and 44.76 m/sec were provided to NASA by Douglas Aircraft. A hot-wire anemometer was used to measure time histories of the vertical component of the tunnel turbulence. Then, by using time-series-analysis techniques on the time-history data, Douglas engineers obtained the psd's over a frequency range of 0 to 50 Hz with a frequency resolution of 0.5 Hz.

To obtain psd's at intermediate tunnel speeds, these psd's were processed further at Langley. It was determined that the areas under the psd's and the maximum values of the psd's varied very closely with the square of tunnel speed. For this reason, the psd's at intermediate tunnel speeds were computed at each frequency using quadratic interpolation based on tunnel speed.

Figure 4 contains log-log plots of the power spectral density functions of the vertical component of tunnel turbulence for tunnel speeds of 30.87, 36.01 and 41.16 m/sec. The psd's are characterized by very pronounced peaks in the neighborhood of 3 Hz. At frequencies above 10 Hz, the psd's drop off roughly with the -5/4 power of frequency. For comparison, the corresponding slopes in the von Kármán and Dryden psd models are -5/3 and -2, respectively.

Data Collection and Reduction

During the turbulence-response wind-tunnel tests, time history responses were obtained from the instrumentation presented in Fig. 2. For each test condition, approximately 200 seconds of data were simultaneously recorded from each instrument on an FM tape recorder. At Langley, the analog tape was digitized at the rate of 250 samples per second. The digitized tape was then processed by a time-series-analysis program (using Fast Fourier Transform techniques) yielding power spectral density functions and the corresponding root-mean-square values (rms's) of each measured response. The frequency range for these psd's was from a low of about 1.5 Hz to a high of 125 Hz, with a frequency resolution of about 0.5 Hz. Because the analytical quantities were computed using the measured tunnel turbulence psd (which was only defined up to 50 Hz), the experimental quantities were recomputed based on an upper frequency limit of 50 Hz.

Normalization

In comparing the system-off turbulence responses for the second and third tunnel tests, some discrepancies were discovered. Whereas torsion responses were repeatable from the second to the third tests, the acceleration response and both bending-moment responses were not repeatable. At the three velocities available for comparison, the bending moment responses differed by a factor of 10 and the acceleration responses differed by a factor of 1.25. This difference suggests errors in the calibration constants from one test to the other. It has not yet been determined which results are in error. Because the problem is unresolved, the absolute values of the experimental response psd's and rms's will not be presented in this paper. Instead, normalized values will be presented. In general, the data will be normalized as follows: (a) for psd's, the value of the psd at a particular response peak will be assigned the normalized value of 1.0, and the other values will be scaled accordingly; (b) for rms's (with the exception of aileron deflection), the value for each response will be normalized by its system-off value; and (c) because the aileron-deflection system-off rms value is zero, it will be normalized by the system-on value at nominal gain and phase. Normalization will have the effect of "removing" any potential calibration errors from the experimental results. If calibration errors are present in the data, they are consistent throughout the test. Therefore, the ratio of two rms values (for example, bending moment system on and system off) which might be "contaminated" by calibration errors would be the same whether they are actually contaminated or not.

Analysis

Predicted turbulence responses for the DC-10 wind-tunnel model were computed using DYLOFLEX, a system of computer programs which performs dynamic loads analyses of flexible airplanes with active controls.[2,3] The equations of motion in DYLOFLEX are formulated through a modal approach using Lagrange's equations of motion. The loads equations in DYLOFLEX are developed using the method of summation of forces. DYLOFLEX requires the following information to perform an analysis: mode shapes, generalized mass and stiffness matrices, lumped masses, static moments and moments of inertia. This information pertaining to the DC-10 wind-tunnel model was supplied to NASA by Douglas Aircraft.

Equations of Motion

In the DYLOFLEX notation the equations of motion are written

$$[M_1]\{q\} + [M_2]\{\dot{q}\} + [M_3]\{\ddot{q}\} + [M_4]\{q\} + [M_5]\{\dot{q}\} = \{C\}\, w_g \qquad (1)$$

where the quantities M_1, M_2, and M_3 are generalized stiffness, damping, and mass matrices, respectively; M_4 and M_5 are generalized aerodynamic matrices due to vehicle motion; C is the generalized aerodynamic column vector due to gust; q is the vector of generalized coordinates (including wing modes, aileron deflection, and active-control-system degrees of freedom); and w_g is the vertical gust velocity. Equation (1) is solved for the generalized coordinates.

Response Equations

The response equations (for bending moment, torsion, acceleration, aileron deflection) are written in terms of the generalized coordinates and their derivatives. The equations for wing bending moment and wing torsion in the DYLOFLEX notation are of the form

$$M_b = \lfloor \bar{M}_3 \rfloor\{\ddot{q}\} + \lfloor \bar{M}_4 \rfloor\{q\} + \lfloor \bar{M}_5 \rfloor\{\dot{q}\} + \bar{C}\, w_g \qquad (2)$$

$$T = \lfloor \bar{\bar{M}}_3 \rfloor\{\ddot{q}\} + \lfloor \bar{\bar{M}}_4 \rfloor\{q\} + \lfloor \bar{\bar{M}}_5 \rfloor\{\dot{q}\} + \bar{\bar{C}}\, w_g \qquad (3)$$

These two responses are each made up of contributions from inertia forces (the terms involving $\ddot{q}$), aerodynamic forces due to vehicle motion (the terms involving q and $\dot{q}$), and aerodynamic forces due to gust (the terms involving w_g). The equation for the acceleration at any location on the wing is

$$\ddot{z} = \lfloor \phi \rfloor\{\ddot{q}\} \qquad (4)$$

where ϕ is the vector of modal deflections at the location where the acceleration is being computed. Because aileron deflection is one of the elements of the generalized coordinate vector, its equation is simply

$$\delta_a = q_j \qquad (5)$$

where q_j is the jth generalized coordinate.

Turbulence Responses

Turbulence responses are predicted in DYLOFLEX using random harmonic analysis techniques. For each of the responses represented by Eqs. (2) through (5), a frequency response function, $H_R(f)$, is computed. (Subscript R represents any of the four responses of interest; f is frequency in Hz.) A response power spectral density function is computed using the frequency response function and the turbulence power spectral density function according to Eq. (6)

$$\Phi_R(f) = \left|H_R(f)\right|^2 \Phi_{w_g}(f) \qquad (6)$$

The quantity $\Phi_{w_g}(f)$ is the tunnel turbulence psd previously discussed and illustrated in Fig. 4 and $\Phi_R(f)$ is the computed response psd. The root-mean-square values (σ_R) of the responses are computed in the following manner

$$\sigma_R = \left[\int_0^{50} \Phi_R(f)\, df\right]^{1/2} \qquad (7)$$

Theoretically, the upper limit of integration in Eq. (7) should be infinity. However, because the tunnel turbulence was only defined to 50 Hz, this value was chosen as the practical upper limit. Because the experimental psd's and rms's will be presented in normalized fashion, the computed quantities will also be normalized. In this manner the experimental and analytical results may be compared directly.

Stability Analyses

All analytical results presented in this paper are for stable systems. To insure that only stable systems were analyzed, stability analyses were performed for many combinations of gain, phase, and velocity. A stability analysis is performed by solving the homogeneous form of Eq. (1) and checking the signs of the real parts of all roots. Though not presented, these rsults are in good agreement with the stability results presented in Ref. 1.

Corrections

The equations of motion in this paper contain an empirical correction factor to modify the theoretically-computed aileron aerodynamic forces. As discussed in Ref. 4, for this wind-tunnel model, theoretically-computed aileron aerodynamic forces are typically 40 percent higher than measured forces. Therefore, the theoretically-computed forces must be multiplied by 0.714 (1/1.4) for them to be on the order of the measured quantities. For reasons of convenience, this 0.714 factor on the aileron forces was incorporated into the analysis in an equivalent manner--by multiplying the feedback gains by 0.714. (For comparison with Ref. 1, a value of K_g of 1.0 in this paper corresponds to a value of 0.714 in Ref. 1.)

As discussed in Ref. 1, a 10° difference was discovered between the measured and computed phase angles at the flutter frequency. This difference had a significant effect on the flutter results and was therefore included in the comparisons of predicted and measured flutter boundaries in Ref. 1. However, in terms of the turbulence-response results, this difference in phase angles had a minimal effect and was therefore not included in this paper.

Comparison of Analytical Predictions and Experimental Results

Analytical and experimental power spectral density functions and root-mean-square values are compared in this part of the paper. The responses which will be compared are wing bending moment at the 48 percent semispan station, wing torsion at the 78 percent semispan station, wing vertical acceleration at the 88 percent semispan station, and (for active-control-system on only) aileron deflection.

Power Spectral Density Functions

System Off. Figure 5 presents normalized psd's of bending moment, torsion, and acceleration for the active-control-system off at 30.87 m/sec. They are presented as log-log plots and each is normalized by its value at the response peak of the first-wing-bending mode (at 6.9 Hz). The analytical and experimental bending-moment psd's show good agreement. Both are characterized by twin peaks at low frequency (tunnel-turbulence peak and first-wing-bending mode) and a prominant peak at about 30 Hz (third-wing-bending mode). A peak at about 15 Hz (second-wing bending) is clearly visible on the experimental psd, but shows up as a barely-distinguishable bump on the analytical psd.

The torsion psd's do not compare as favorably. The peaks of all modes do occur at the correct frequencies, but the magnitudes differ, especially at the tunnel-turbulence peak (about 3 Hz) and at the peak at about 40 Hz (second-wing torsion). Both peaks are underpredicted analytically. This underprediction is emphasized by the fact that the maximum value of the experimental torsion psd occurs at the second-torsion peak.

The acceleration psd's agree more favorably. The analytical and experimental psd's agree very well through the second-bending peak at about 15 Hz. However, the second-wing-torsion peak at about 40 Hz is again significantly underpredicted by analysis.

System On. Figure 6 presents normalized psd's of bending moment, torsion, acceleration and aileron deflection for the active-control-system on (K_g = 1.0, ϕ = 0°) at 30.87 m/sec. With the exception of the aileron-deflection psd (which did not appear in Fig. 5), all psd's are normalized to their system-off values at the first-wing-bending peak. The aileron-deflection psd's are normalized by their values at the system-on first-bending peak, now at a frequency of 10.9 Hz. Because the ACS is on, the character of the psd's have changed as compared to those in Fig. 5. The analysis predicted these changes well. The peak at about 3 Hz is now due to not only the tunnel turbulence, but also due to an ACS filter mode at almost the same frequency. The result is an increase in the magnitude of those peaks compared to system off. This increase was predicted analytically and verified experimentally. Another change as compared to Fig. 5 was an increase in the frequency (from 6.9 to 10.9 Hz) and a significant reduction in the magnitude of the first-bending peak. The reductions are clearly illustrated by comparing the magnitude of the peak with the horizontal dashed line (which represents the magnitude of the first-bending peak for system off).

Comparing the analytically-predicted and experimental psd's within Fig. 6, the response peaks occur at the same frequencies. As was the case for the system-off psd's, the flutter mode shows up analytically (as a spike at 12.3 Hz) but not experimentally, and the second-torsion peak is underpredicted analytically.

Variation of ACS Parameters. When considering gust load alleviation, bending moment is the load of primary interest. From Figs. 5 and 6 (from system off to system on) there is a significant reduction in the area under the bending moment psd. This reduction indicates that this active control system, although designed for the purpose of flutter suppression, is also effective in alleviating gust loads at nominal values of gain and phase. Thus, from a gust-load-alleviation point of view, it is of interest to investigate the effects on the bending moment of varying ACS parameters K_g and ϕ.

Figure 7 presents analytically-predicted and experimental normalized bending-moment psd's for four values of gain, K_g. Starting at zero, K_g increases from left to right in increments of 0.5. Phase angle, ϕ, is zero for each plot. The vertical scales are again normalized to the system-off peak value of the first-bending mode. As gain increases from 0 to 1.5, the analysis correctly predicts the following changes in the bending-moment psd: the frequency of the first-bending mode increases by almost a factor of two (from 6.9 Hz to 12.3 Hz); and the magnitude of the first-bending peak decreases by one and one-half (1-1/2) orders of magnitude. The analysis also correctly predicts a small increase in the magnitude of the low-frequency tunnel-turbulence/filter peak (at about 3 Hz).

Figure 8 presents normalized bending-moment psd's for values of phase angle, ϕ, of -10^o, 0^o 20^o, and 40^o. The normalization in this figure is the same as that in Fig. 7. Gain, K_g, is unity for each plot. The analysis correctly predicts the trends with increasing phase angle. For both analysis and experiment, the psd's for $\phi = -10^o$ and $\phi = 0^o$ are almost identical, with the first-bending peak at 10.9 Hz. With increasing phase angle, the first-bending frequency again increases, resulting, again, in a reduction in magnitude of the first-bending peak. At the same time, the magnitude of the low-frequency peak increases. This increase is attributed to decreased damping in the filter mode. At $\phi = 40^o$, as compared to experiment, the analysis overpredicts the magnitude of the filter peak. This overprediction is a consequence of the analysis underpredicting the damping in the filter mode. With further-increasing phase angle, the analysis predicts an instability in the filter mode. It is believed that the analysis predicts this instability at a lower value of ϕ than experiment would indicate. Therefore, 40^o would be "closer" to the instability analytically than it would be experimentally, resulting in lower damping and a considerably higher response peak.

Root Mean Square Values

Figure 9 presents comparisons of analytically-predicted and experimental normalized rms values of bending moment, torsion, acceleration, and aileron deflection for variations in the ACS parameters. The first three quantities are normalized by their system-off rms values. Aileron deflection is normalized by its rms value at nominal gain and phase. The normalized rms's are plotted as a function of gain for the four values of phase considered in Fig. 8. In addition to computing rms's at the four values of gain for which experimental data were available (and considered in Fig. 7), they were also computed at intermediate gains of 0.25, 0.75, and 1.25. Analytical results are plotted as open symbols and experimental results are plotted as closed symbols. For all four responses, the system-off condition is represented by the value at $K_g = 0$.

Figure 9a illustrates the variation in normalized bending-moment rms values with gain and phase. For all gains, at $\phi = -10°$ and $\phi = 0°$, the values of the analytical rms's are so nearly equal as to be almost coincident on the plot. This result is verified experimentally by the closeness of the closed circle and triangle symbols at each gain. For $\phi = -10°$ and $\phi = 0°$, the normalized bending moment decreases with increasing gain, up to reductions of about 20 percent at $K_g = 1.0$ and 30 percent at $K_g = 1.5$. Referring back to the bending-moment psd's in Fig. 7, this reduction in rms value is due to the large reduction in the area under the peak of the first-bending mode. For $\phi = 20°$ and $\phi = 40°$ in Fig. 9a, the normalized rms increases, both analytically and experimentally, with increasing K_g. At gain $K_g = 1.0$ in Fig. 9a, the rms value increases with increasing phase angle. Referring back to the bending-moment psd's in Fig. 8, this increase is due to the large increase in the area under the peak of the filter mode.

Figures 9b and 9c contain comparisons for torsion and acceleration, respectively. The agreement between analysis and experiment for these two responses is not as good as it was for bending moment and is, in part, due to the analysis underpredicting the second-torsion peak in both the torsion and the acceleration psd's. The experimental torsion and acceleration data are almost insensitive to variations in both gain and phase angle. In addition, unlike the case of bending moment, there appear to be no distinguishable consistent trends in the experimental data for these two responses. Work is continuing to explain the differences between analysis and experiment.

Figure 9d contains comparisons for aileron deflection. Inspection of the figure indicates good agreement between analysis and experiment. For all gains, the normalized rms values show only small differences from $\phi = -10°$ to $\phi = 0°$, but increase significantly with increasing phase angle. For all phase angles, the rms values increase with increasing gain.

Experimental data were also collected at tunnel speeds up to 41.16 m/sec. However, because of visibly larger wing deflections and the fear of damaging the model, at the higher tunnel speeds, turbulence-response data were collected at fewer combinations of gain and phase. Figure 10 presents comparisons of normalized bending-moment rms values at 36.01 and 41.16 m/sec, respectively. In this figure, analytical results are only presented for values of phase angle at which experimental data were obtained: three phase angles were tested at 36.01 m/sec and two phase angles were tested at 41.16 m/sec. The analytical results presented in Fig. 10a for $\phi = -10°$ and $\phi = 0°$ were virtually identical. Once again, the experimental data verified this result. The "gap" in Fig. 10b for the zero-phase-angle analytical data is due to a predicted instability at gains of 0.50 and 0.75. At both 36.01 and 41.16 m/sec, the trends with increasing gain and phase are predicted very well by the analysis.

Concluding Remarks

Turbulence responses of a wind-tunnel model of a DC-10 derivative wing were obtained experimentally and computed analytically. The model was aeroelastically scaled and was equipped with a NASA-developed active control system. The experimental turbulence responses were obtained by performing time series analyses on measured time histories of several model responses. The analytical turbulence responses were obtained using a computer program which performs dynamic loads

analyses of flexible airplanes equipped with active control systems (DYLOFLEX).

The wind-tunnel tests afforded the opportunity to validate the analysis method by comparing the analytical predictions with the measured turbulence responses. Tunnel speed and control-system gain and phase were varied systematically during the tests and the following responses were compared: wing bending moment, wing torsion, wing acceleration, and aileron deflection. The analysis predicted well the variations of bending moment and aileron deflection with active-control-system parameters. Experimental torsion and acceleration responses exhibited low sensitivity to variations in gain and phase angle and did not compare as well with the analytically-predicted trends. This result is puzzling in light of the favorable agreement, at the same test conditions, for the other two responses.

Of particular interest is the result that the NASA active control system (designed for the purpose of flutter suppression only) is also effective in reducing wing bending moments due to gust. For both analytical predictions and experiment, at nominal values of gain and phase, the active control system reduced wing bending moments approximately 25 percent over a range of tunnel speeds.

Acknowledgement

The author wishes to acknowledge the work of E. Tescher, J. Nomura, J. Schlama, and A. Shirley of the McDonnell Douglas Corporation. The successful completion of this study was due largely to their skillful efforts in conducting the wind-tunnel tests and acquiring the experimental data.

References

[1]Abel, I.; and Newsom, J. R.: Wind-Tunnel Evaluation of NASA-Developed Control Laws for Flutter Suppression on a DC-10 Derivative Wing. AIAA Paper No. 81-0639. Presented at AIAA Dynamics Specialists Conference, Atlanta, GA, April 1981.

[2]Perry, B., III; Kroll, R. I.; Miller, R. D.; and Goetz, R. C.: DYLOFLEX: A Computer Program for Flexible Aircraft Flight Dynamic Loads Analyses with Active Controls. J. Aircraft, Vol. 17, No. 4, pp. 275-282, April 1980.

[3]Miller, R. D.; Kroll, R. I.; and Clemmons, R. E.: Dynamic Loads Analysis System (DYLOFLEX) Summary. NASA CR-2846-1, September 1979.

[4]Winther, B. A.; Shirley, W. A.; and Heimbaugh, R. M.: Wind Tunnel Investigation of Active Controls Technology Applied to a DC-10 Derivative. AIAA Paper No. 80-0771. Presented at AIAA/ASME/ASCE/AHS 21st Structures, Structural Dynamics, and Materials Conference, Seattle, WA, May 1980.

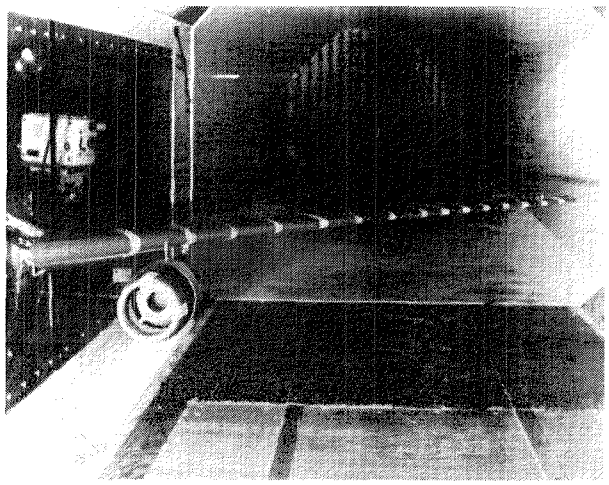

Fig. 1 Photograph of model in wind tunnel.

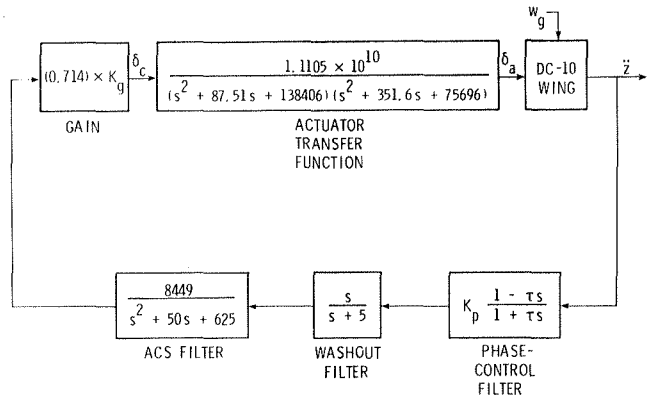

Fig. 3 Block diagram of active control system.

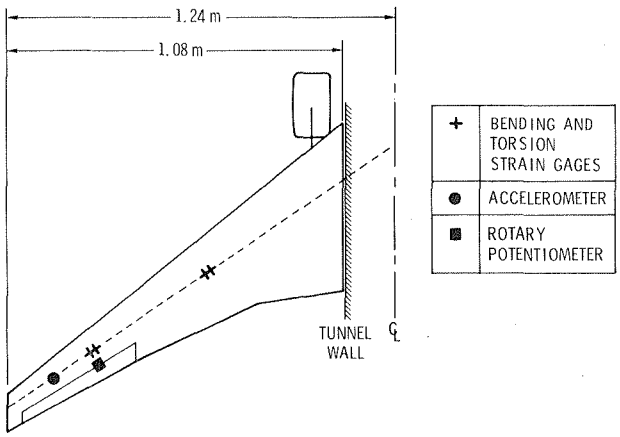

Fig. 2 Model instrumentation.

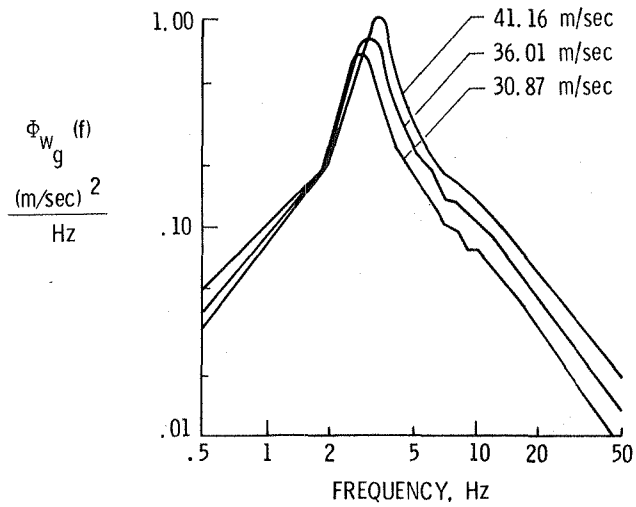

Fig. 4 Power spectral density functions of the vertical component of wind-tunnel turbulence for three tunnel speeds.

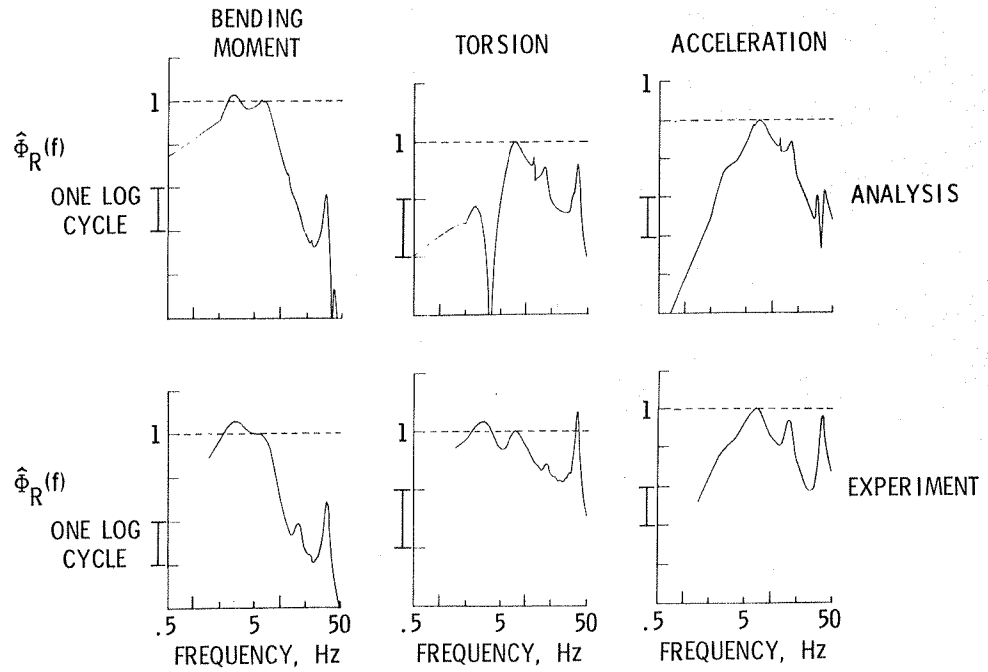

Fig. 5 Normalized power spectral density functions. System off; 30.87 m/sec.

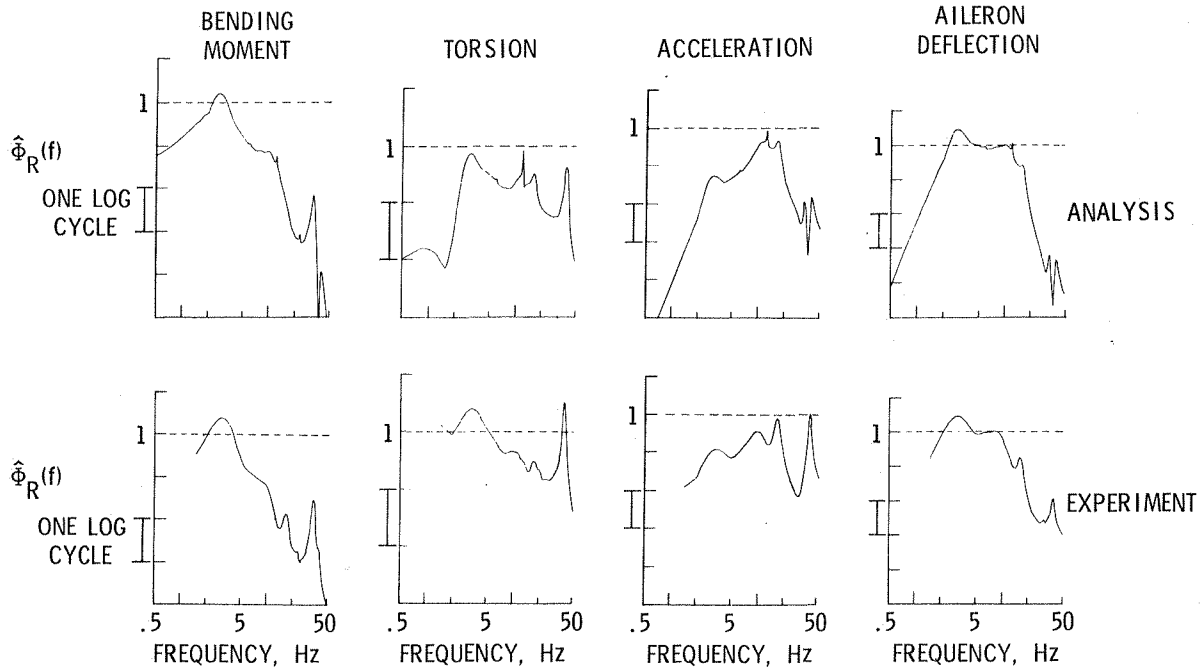

Fig. 6 Normalized power spectral density functions. System on, K_g = 1.0, $\phi = 0^o$; 30.87 m/sec.

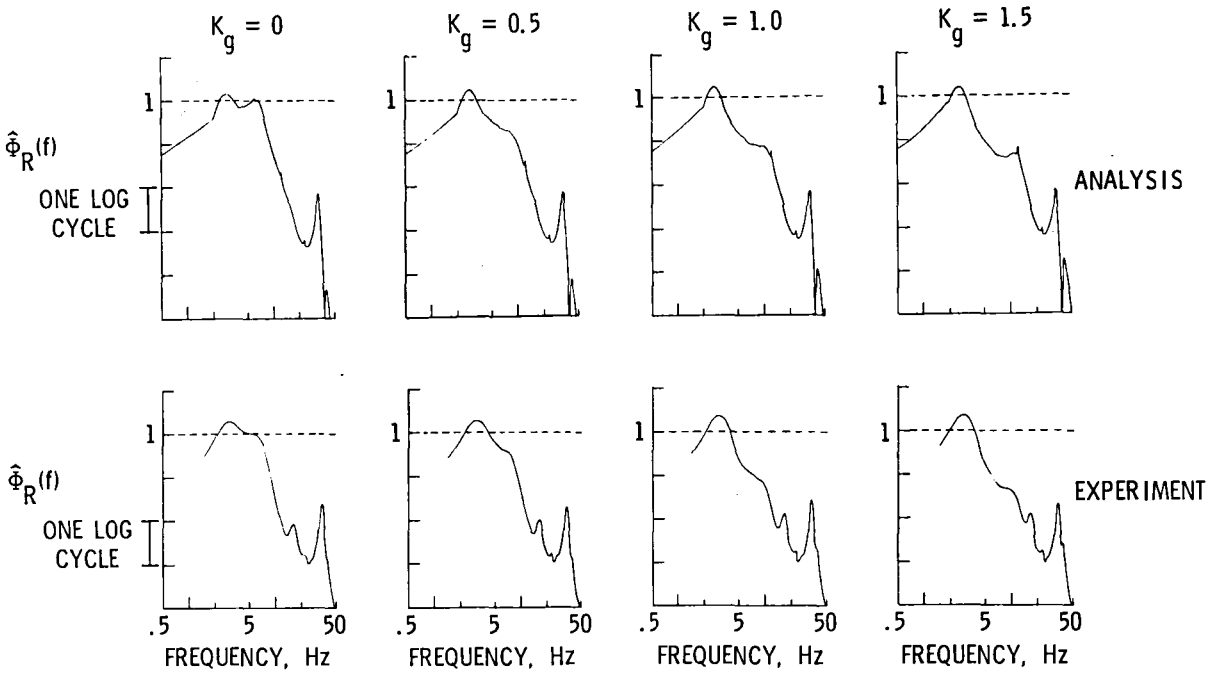

Fig. 7 Normalized bending-moment psd's as a function of gain. System on, $\phi = 0^o$; 30.87 m/sec.

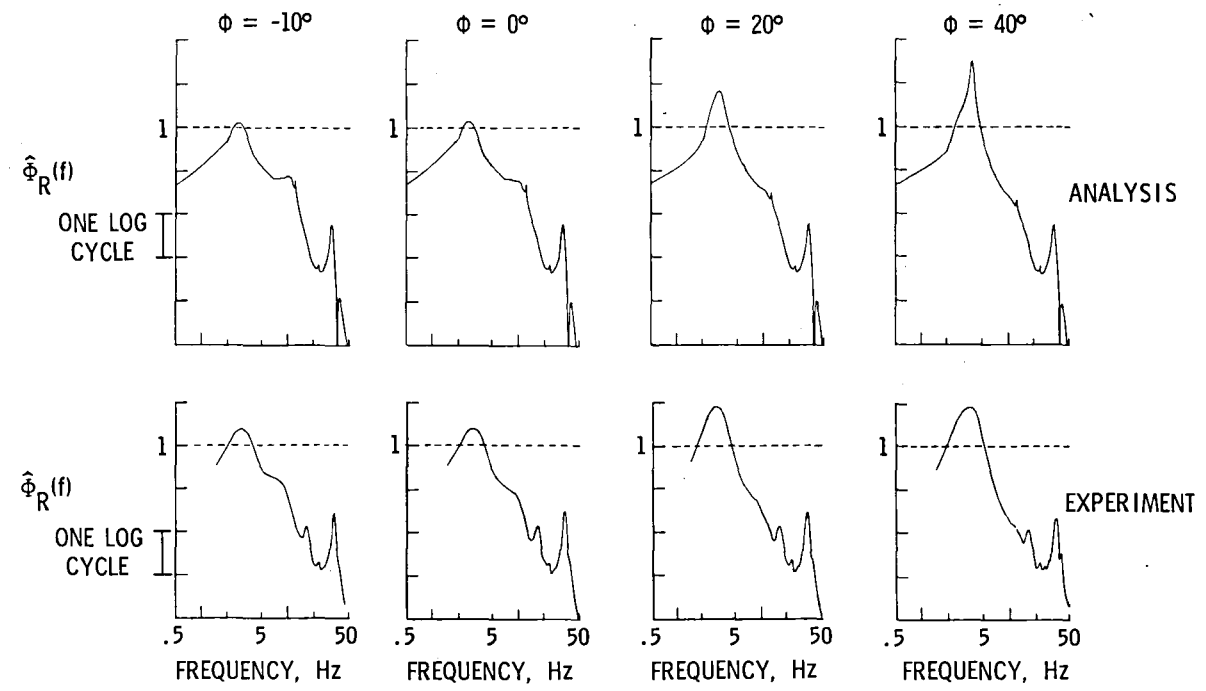

Fig. 8 Normalized bending-moment psd's as a function of phase angle. System on, $K_g = 1.0$; 30.87 m/sec.

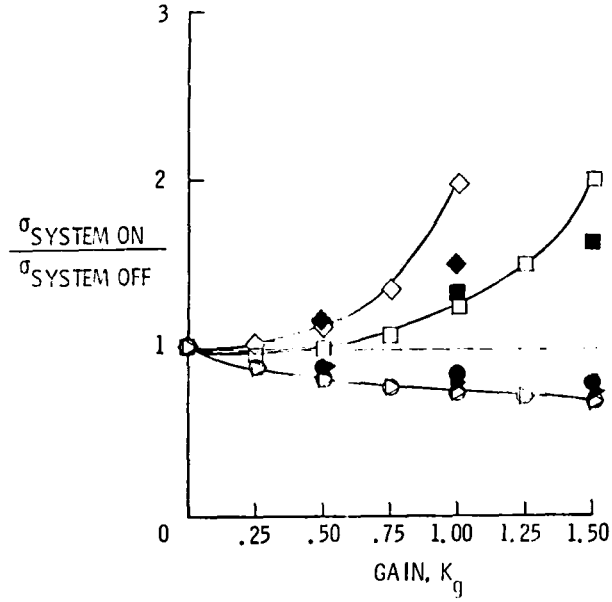

(a) Bending moment

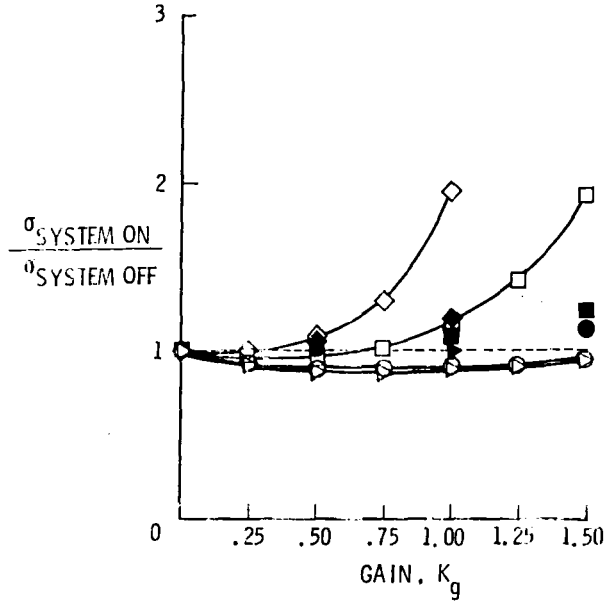

(b) Torsion

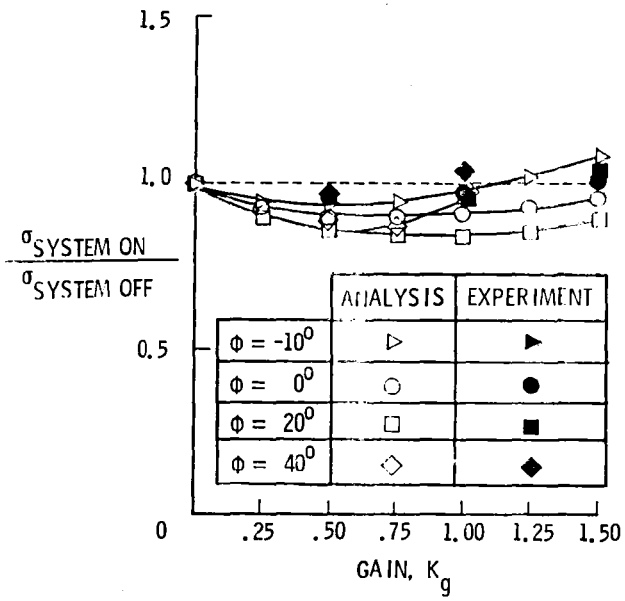

(c) Acceleration

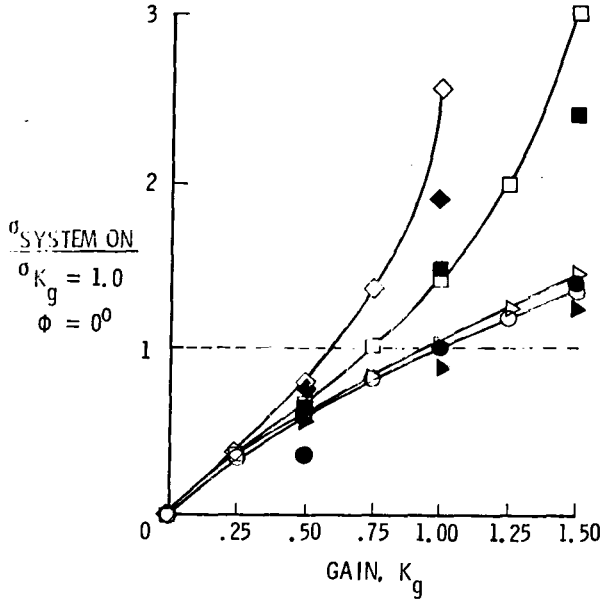

(d) Aileron deflection

Fig. 9 Comparison of normalized turbulence responses at 30.87 m/sec.

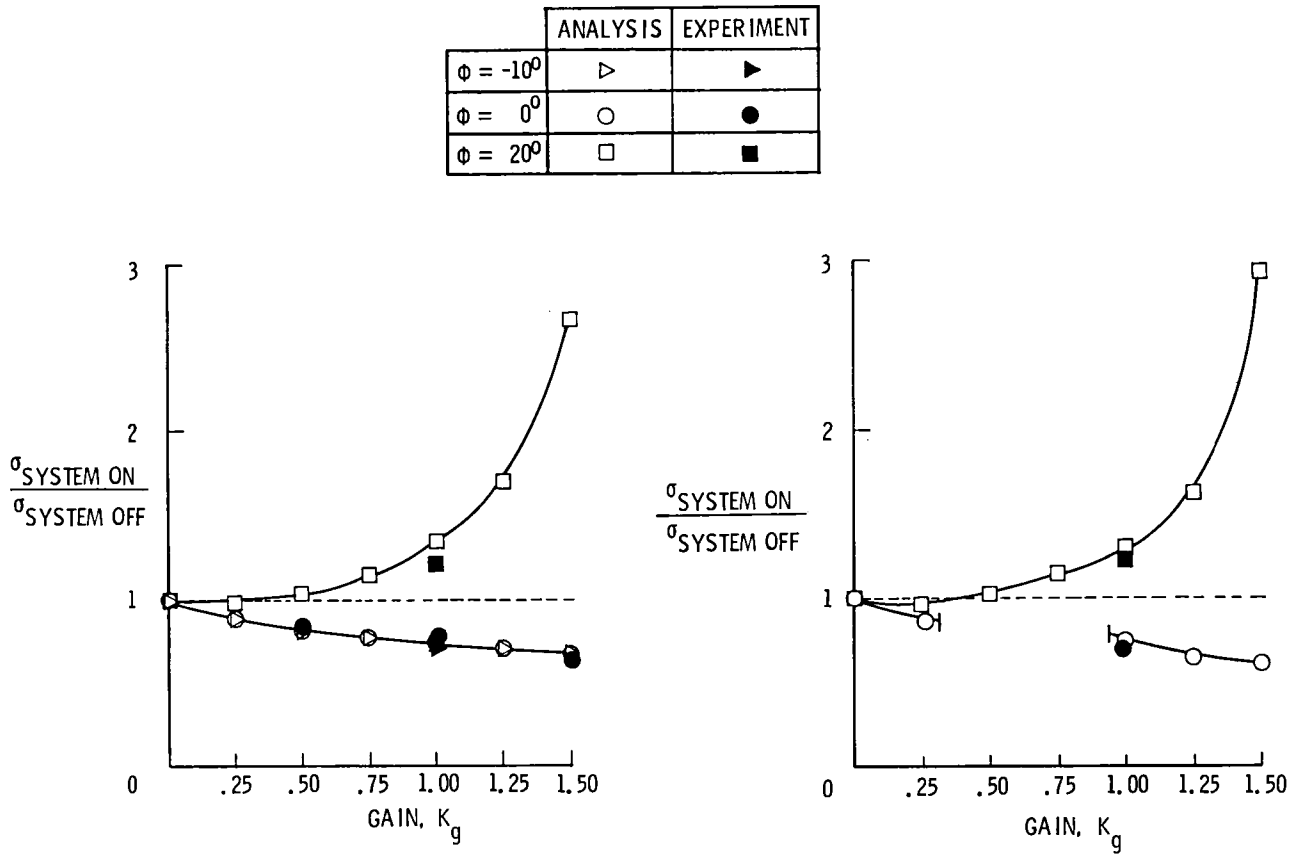

(a) 36.01 m/sec

(b) 41.16 m/sec

Fig. 10 Comparison of normalized bending-moment turbulence responses.

1. Report No.	2. Government Accession No.	3. Recipient's Catalog No.
NASA TM-83144		

4. Title and Subtitle	5. Report Date
Qualitative Comparison of Calculated Turbulence Responses With Wind-Tunnel Measurements for a DC-10 Derivative Wing With an Active Control System	June 1981
	6. Performing Organization Code: 505-33-63-02

7. Author(s)	8. Performing Organization Report No.
Boyd Perry, III	

9. Performing Organization Name and Address	10. Work Unit No.
NASA Langley Research Center Hampton, Virginia 23665	11. Contract or Grant No.

12. Sponsoring Agency Name and Address	13. Type of Report and Period Covered
National Aeronautics and Space Administration Washington, DC 20546	Technical Memorandum
	14. Sponsoring Agency Code

15. Supplementary Notes

Presented at the AIAA Dynamics Specialist Conference, Atlanta, Georgia, April 8-11, 1981. AIAA Paper No. 81-0567.

16. Abstract

This paper presents comparisons of analytically-predicted and experimental turbulence responses of a wind tunnel model of a DC-10 derivative wing equipped with an active control system. The active control system was designed for the purpose of flutter suppression, but it had the additional benefit of alleviating gust loads (wing bending moment) by about 25 percent. Comparisons of various wing responses are presented for variations in active-control-system parameters and tunnel speed. The analytical turbulence responses were obtained using DYLOFLEX, a computer program for dynamic loads analyses of flexible airplanes with active controls. In general, the analytical predictions agreed reasonably well with the experimental data.

17. Key Words (Suggested by Author(s))	18. Distribution Statement
Turbulence responses Active controls DYLOFLEX	Unclassified - Unlimited Subject Category 39

19. Security Classif. (of this report)	20. Security Classif. (of this page)	21. No. of Pages	22. Price
Unclassified	Unclassified	12	A02

For sale by the National Technical Information Service, Springfield, Virginia 22161

End of Document